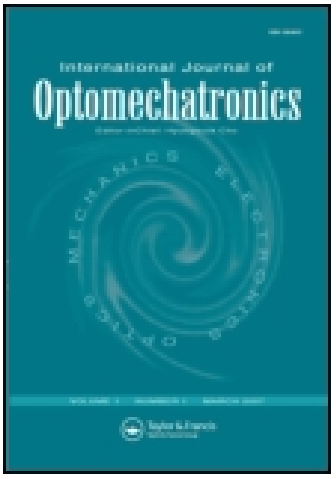

International Journal of Optomechatronics
Publication details, including instructions for authors and subscription information:
http://www.tandfonline.com/loi/uopt20

A Controller Design for Precision Laser-Beam Positioning System

Youngtae Woo [a] & Young Chol Kim [b]
[a] Department of Electronic Engineering , Chungbuk National University , Cheong-ju, Korea
[b] School of Electrical & Electronic Engineering, Chungbuk National University , Cheong-ju, Korea
Published online: 09 Jun 2011.

To cite this article: Youngtae Woo & Young Chol Kim (2011) A Controller Design for Precision Laser-Beam Positioning System, International Journal of Optomechatronics, 5:2, 107-127, DOI: 10.1080/15599612.2011.581740

To link to this article: http://dx.doi.org/10.1080/15599612.2011.581740

International Journal of Optomechatronics, 5: 107–127, 2011

ISSN: 1559-9612 print/1559-9620 online
DOI: 10.1080/15599612.2011.581740

Taylor & Francis
Taylor & Francis Group

A CONTROLLER DESIGN FOR PRECISION LASER-BEAM POSITIONING SYSTEM

Youngtae Woo[1] and Young Chol Kim[2]
[1]*Department of Electronic Engineering, Chungbuk National University, Cheong-ju, Korea*
[2]*School of Electrical & Electronic Engineering, Chungbuk National University, Cheong-ju, Korea*

This article presents a decentralized control strategy for a two-axis precision laser-beam positioning system (PLPS). The PLPS is composed of two integrated subsystems: the telescope system equipped with a FSM platform and the beam alignment system. The strategy included actual data acquisition, system analysis and modeling, digital controller design, and experimental evaluations. The controller had a sensitivity margin of less than −10 dB at 20 Hz on each axis, and maintained the stability of PLPS. The system had moderate robustness, tracked the command signals and output responses without steady-state errors.

Keywords: beam alignment system, decentralized digital controller, K-polynomial, partial model matching method, precision laser-beam positioning system

1. INTRODUCTION

The laser was used restrictively in scientific research and military weapons until the 1990s extended its usefulness to a variety of other applications including data storage, the complicated optical systems used for tactical high energy laser (Schwartz et al. 2002), and free-space optical communication (Skormin et al. 1995). Sweeney et al. (2002) presented an actual design of a fast steering mirror (FSM) and its performance data in the free space laser telecom system and discussed the mechanical tradeoffs among the range of motion and other structures. Based on the principle of laser-beam reflection, the rapid development of its numerous applications has increasingly demanded the precise optical alignment for the laser-based optical systems.

The PLPS has been developed to accurately measure laser deformation from the desired optical axis. Moreover, its working performance mainly relies on the extent that orthogonal displacements of the laser are minimized. The success of a laser-beam positioning mechanism in PLPS depends on the ability of the laser beam to hold its properties over long distances without deviations and be focused into specified spots uniformly.

Address correspondence to Young Chol Kim, School of Electrical & Electronic Engineering, Chungbuk National University, Gaesin-dong 12, Cheong-ju, Korea. E-mail: yckim@cbu.ac.kr

NOMENCLATURE

$G_{PLPS}(s)$	model of the PLPS	$S_i(s)$ $(i=x, y)$	sensitivity transfer functions
$G_{ij}(s)$ $(i, j=1, 2)$	transfer function elements of $G_{PLPS}(s)$	$T_i^*(s)$ $(i=x, y)$	target closed-loop transfer functions
$\widehat{G}_{ij}$ (s) $(i, j=1, 2)$	identified model of G_{ij} (s)	δ_i^* $(s)(i=x, y)$	target characteristic polynomials
$W(i)$	weighting sequence		
P	weighted least square estimation (LSE) of parameters of $\widehat{G}_{ij}$ (s)	$f_0(x)$	cost function in the partial model matching (PMM) problem
K_{ij} $(i, j=1, 2)$	steady-state gains of the transfer functions, G_{ij} (s)	x_o^*, x^*	continuous-time controller gains and the optimized controller gains in PMM problem
λ_{ij} $(i, j=1, 2)$	relative gain array (RGA) matrix	α_i	characteristic ratios
F_i (s) $(i=x, y)$	continuous-time notch filters	τ	generalized time constant
C_i (s) $(i=x, y)$	continuous-time controllers	A_D, B_D, C_D, D_D	gains of the digital controller
T_i (s) $(i=x, y)$	closed-loop transfer functions	$NF(z)$	discrete form of the notch filter
δ_i (s) $(i=x, y)$	characteristic polynomials		

It is important to study the precision of laser-beam positioning. A finer solution and better performance of PLPS can provide the accurate and stable laser-beam steering for fast response characteristics of the active mirrors and maintaining the alignment. PLPS can contribute to the robustness of the optical systems, when we consider the challenging environments due to structural stress, vibrations, and drifts. A very small angular displacement of the laser-beam can induce significant beam position errors when amplified by the undesirable disturbances.

As a solution to cope with the undesirable environments, Orzechoski et al. (2008a) employed an adaptive controller to achieve minimum output-error variance in terms of suppression of jitter in the laser-beam steering system. Moreover, Orzechoski et al. (2008b) also demonstrated the capabilities of the new liquid crystal device and an adaptive controller to suppress high-bandwidth jitter. Thus efforts to overcome those variations by correcting for the misalignment on the optical axis may enhance the beam stabilization and system performance.

The purpose of this article is to design a controller so that the PLPS has the ability to track the command signals quickly and reject undesirable disturbances. As one of the most important design specifications, the sensitivity of the overall system should be less than -10 dB at 20 Hz on the two axis. Also the controller should achieve a good transient response within a given control input limitation on both axes and a sampling frequency of 3 kHz. Furthermore, PLPS itself is regarded as the subject to complete the described control objectives. Our approach is different from others (Zhou et al. 2009; Kuang et al. 2009) in that we consider the whole system of PLPS instead of a restrictive module, such as a FSM in its structure as a control object.

This article has five other sections. Section 2 includes descriptions of the PLPS and a problem formulation. In Section 3, some details on data acquisition and model identification of the PLPS are given, along with a multivariable analysis on the identified model of PLPS. Section 4 describes the controller design for achieving

good disturbance rejection by using the partial model matching (PMM) method. Section 5 provides the experimental results and evaluations. Finally, in Section 6, the conclusion follows.

2. OUTLINE OF THE PLPS AND PROBLEM FORMULATION

The PLPS dealt with in this article is a mechanical assembly with two integrated subsystems: the telescope system equipped with a FSM platform and the beam alignment system. Also, several reflecting mirrors including FSM link two subsystems by performing the laser-beam delivery from the source to a target. Figure 1 illustrates the overall structure of PLPS and its operational mechanism. Next, details of both systems are provided.

The telescope system consists of a lightweight primary mirror with a secondary mirror, and it plays a role of guiding the laser beam to specified points. In its structure, an FSM platform is located for the purpose of allowing the attached mirror to have high-dynamic and precise movements in two orthogonal axes with a pivot point. The dynamic behavior of the platform for laser-beam positioning is determined by the tip/tilt movement of FSM mounted over the piezoelectric actuators controlled differentially in pairs.

As for the beam alignment system, it is comprised of three components: 1) a beam splitter for separating an incident laser-beam into two beams, one reflected and the other transmitted, 2) a beam expander for collimating a Helium-Neon (He-Ne) laser used for beam alignment test and 3) a position sensing detector (PSD) for measuring the displacements of the laser-beam off the central point. This composition is critical in designing a controller to perform the compensation of beam position errors and the beam alignment.

Before using a high energy laser, a He-Ne laser is discharged to the PLPS as a test source. It travels to and fro between beam alignment system and the telescope. The beam reflected back from FSM in the telescope arrives at PSD. The signals from PSD are then sent to the digital signal processor (DSP) controller unit. The process

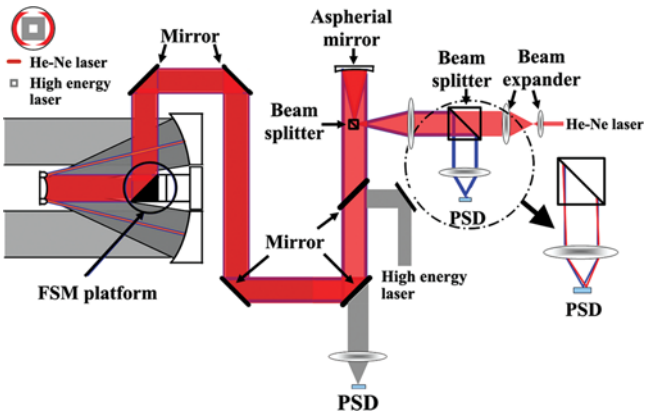

Figure 1. Schematic diagram of precision laser-beam positioning system.

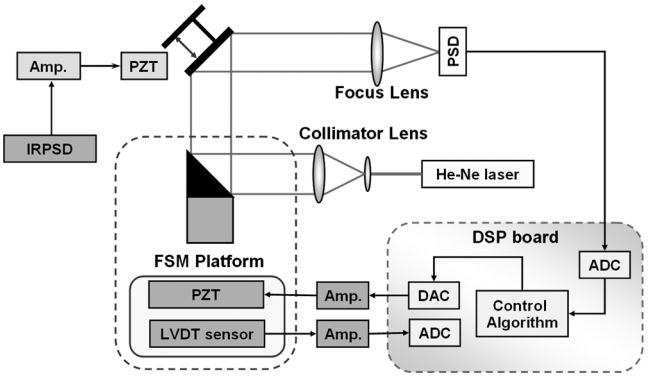

Figure 2. Hardware configuration for the PLPS.

accounts for a way to obtain the electric signals which represent beam position errors in the closed-loop operation. In the end, the digital controller implemented on DSP module generates the command signal for the compensation of misalignment. Figure 2 illustrates the simplified hardware configuration for PLPS.

For the two-axis PLPS, we consider the two-parameter feedback control structure in each loop as shown in Figure 3. The definitions in Table 1 denote all the symbols in Figure 3. Herein, we assumed that the model of PLPS is considered as a 2×2 linear multivariable system and its nonlinearity is negligible.

Let the model of the PLPS be

$$G_{PLPS}(s) = \begin{bmatrix} G_{11}(s) & G_{12}(s) \\ G_{21}(s) & G_{22}(s) \end{bmatrix}. \tag{1}$$

The main purpose is to develop a digital controller that has the ability to reject disturbances. In particular, the sensitivity of the overall system should be less than -10 dB at 20 Hz on both axes. The controller is required to achieve a good transient response as well. In order to achieve these objectives, we try to find such a controller using the decentralized control design instead of a multivariable control approach.

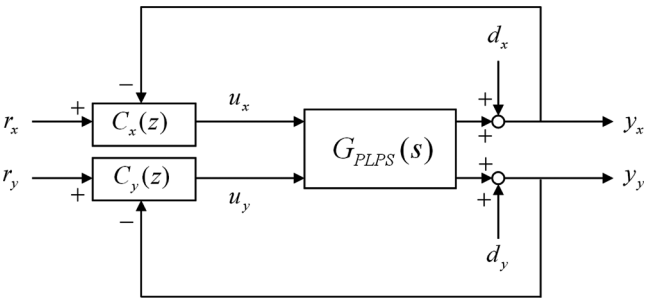

Figure 3. Block diagram of the control system with the PLPS.

Table 1. Symbol and notations

Notation	X axis		Y axis
Command signal (IRPSD)	r_x		r_y
Control input signal	u_x		u_y
Output signal (PSD)	y_x		y_y
Disturbance signal	d_x		d_y
Plant (PLPS)		$G_{PLPS}(s)$	
Digital controller	$C_x(z)$		$C_y(z)$

3. MODELING AND ANALYSIS ON PLPS

3.1. Frequency Response Data Acquisition

The first step in the control strategy involves measuring the frequency response data set from the two-axis PLPS by using an Agilent 35670A Dynamic Signal Analyzer. For the model, represented by a 2×2 transfer function matrix as described in equation (1), it is necessary to obtain the four corresponding frequency response data.

With these considerations in mind, we excited the PLPS with a sinusoidal waveform with $\pm 0.5 V_{pp}$ at a sweeping frequency of 1 Hz $\sim$ 1 kHz, and then measured the magnitude (in dB) and phase (in degrees) of the responses. On the basis of a series of laboratory tests, reliable response data of the PLPS were collected.

3.2. System Identification and Analysis on PLPS

The frequency response data obtained experimentally are shown in Figure 4 and Figure 5. After conducting several model validity tests, we have determined that the proper orders of all $G_{ij}(s)$, $i, j = 1, 2$ are (degree of numerator/degree of denominator) $= 3/6$. That is,

$$\widehat{G}_{ij}(s) = \frac{\widehat{N}_{ij}(s)}{\widehat{D}_{ij}(s)} = \frac{b_3 s^3 + b_2 s^2 + b_1 s + b_0}{s^6 + a_5 s^5 + \cdots + a_1 s + a_0}, \tag{2}$$

where $i, j = 1, 2$. Then, we used the least square estimation (LSE) to identify the coefficients in equation (2). Here, 381 valid points of the responses for $\widehat{G}_{22}(s)$ were used and 341 points for $\widehat{G}_{11}(s)$, $\widehat{G}_{12}(s)$, $\widehat{G}_{21}(s)$.

We define the magnitude and phase responses of $G_{ij}(s)$ as Ap_i and ϕp_i, respectively. Then for a frequency ω_i, we have

$$Ap_i \cos \phi p_i + jAp_i \sin \phi p_i = \frac{b_3(-j\omega_i^3) + \cdots + b_1(j\omega_i) + b_0}{-\omega_i^6 + a_5(j\omega_i^5) + \cdots + a_1(j\omega_i) + a_0}, \tag{3}$$

where i is the data sequence index. By equating the real and imaginary parts on both sides of (3) and rearranging the terms, we obtain

$$X_i P = Y_i, \tag{4}$$

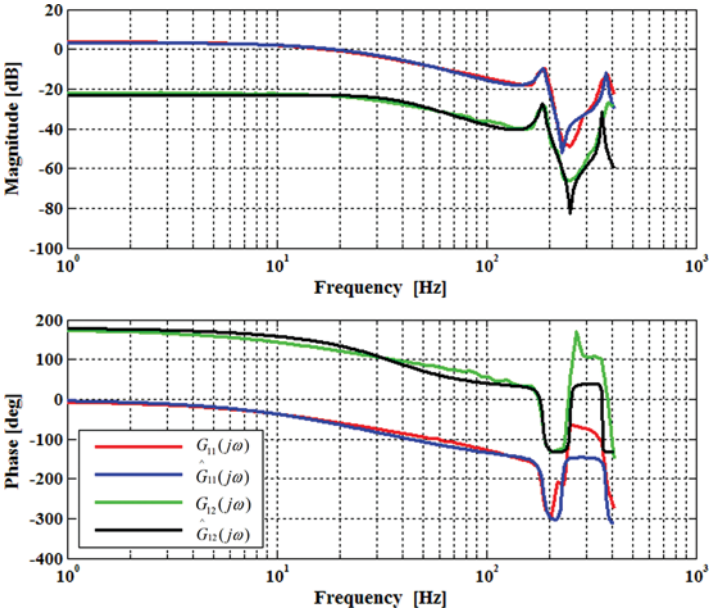

Figure 4. Bode plots of open-loop system and model validations for $G_{11}(s)$ and $G_{12}(s)$.

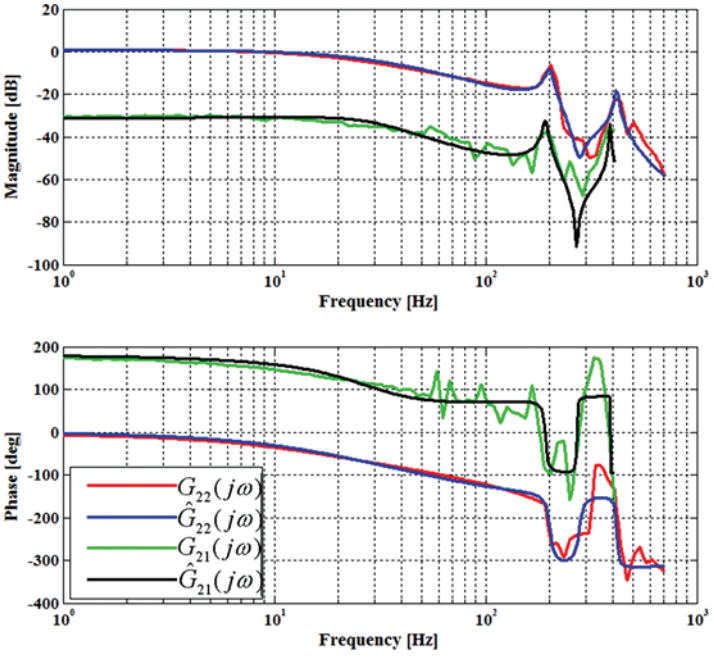

Figure 5. Bode plots of open-loop system and model validations for $G_{21}(s)$ and $G_{22}(s)$.

where

$$X_i = \begin{bmatrix} -\omega_i^5 A p_i \sin\phi p_i & \cdots & 0 & -1 \\ \omega_i^5 A p_i \cos\phi p_i & \cdots & -\omega_i & 0 \end{bmatrix},$$
$$P = [\, a_5 \quad \cdots \quad a_0 \quad b_3 \quad \cdots \quad b_0 \,]^T,$$
$$Y_i = [\, \omega_i^6 A p_i \cos\phi p_i \quad \omega_i^6 A p_i \sin\phi p_i \,]^T.$$

Therefore, the LSE solution for all data sequences is given by

$$P = (X^T X)^{-1} X^T Y, \tag{5}$$

where

$$X = [\, X_1^T \quad X_2^T \quad \cdots \quad X_i^T \,]^T,$$
$$Y = [\, Y_1^T \quad Y_2^T \quad \cdots \quad Y_i^T \,]^T.$$

To improve the accuracy of the parameter estimation, the following weighting sequence was taken into account:

$$W(i) = \frac{1}{(1-\gamma)\gamma^{N-\delta}} \quad \text{for} \quad \gamma < 1, \tag{6}$$

where γ is a weighting constant, N is the number of data, and $\delta$is the weighting index. The factor γ is related to the reduction of the noise effects and δ is the time observations (Franklin et al. 1997). By combining equations (5) and (6), the weighted LSE solution is obtained which is given by

$$P = (X^T W(i) X)^{-1} X^T W(i) Y. \tag{7}$$

In equation (7), it is clear that the proper weighting sequence should be decided to identify a reliable model of PLPS. So we divided the frequency response data into four corresponding intervals represented by A, B, C and D in Figure 4. Then we assigned the proper weighted values on the weighted LSE according to the magnitudes and the sizes of the data.

In Figure 4 and Figure 5, the responses of the identified models and experimental responses data are shown for the sake of comparison. Also the parameters of the identified models are described in the Appendix. The identified models represent the minimum phase transfer functions.

3.3. RGA (Relative Gain Array) Analysis on PLPS

Once the multivariable model of PLPS has been established, the existence and extent of the interactions between the models need to be analyzed before we deal with decentralized control. The relative gain array (RGA) introduced by (Bristol 1996) gives an analytical insight into the selection of the manipulative-controlled variable-pairings. It is also used to predict the behavior of the controlled responses (Shinsky 1981).

Let us define a steady-state model for PLPS as follows:

$$\begin{aligned} y_x &= K_{11}u_x + K_{12}u_y \\ y_y &= K_{21}u_x + K_{22}u_y, \end{aligned} \tag{8}$$

where K_{ij} $(i, j = 1, 2)$ are the steady-state gains of the transfer functions in equation (1).

Then the calculated steady-state gain matrix is given by

$$K_{ij} = \begin{bmatrix} 1.44641 & -7.95380 \times 10^{-2} \\ -2.83913 \times 10^{-2} & 1.08425 \end{bmatrix}. \tag{9}$$

By definition (Bristol 1996), the RGA matrix for the 2×2 model is

$$\lambda = \begin{bmatrix} \lambda_{11} & \lambda_{12} \\ \lambda_{21} & \lambda_{22} \end{bmatrix} = \begin{bmatrix} \lambda_{11} & 1 - \lambda_{11} \\ 1 - \lambda_{11} & \lambda_{11} \end{bmatrix}, \tag{10}$$

where $\lambda_{11} = \frac{1}{1-(K_{12}K_{21})/(K_{11}K_{22})}$. Based on equations (9) and (10), the RGA matrix is given by

$$\lambda = \begin{bmatrix} 1.00144 & -1.44198 \times 10^{-3} \\ -1.44198 \times 10^{-3} & 1.00144 \end{bmatrix}. \tag{11}$$

The values of λ_{12} and λ_{21} suggest that the interactions are negligible. If we extend this analysis to the case of bending modes having the natural frequencies, then similar results can be obtained. For the first and second natural frequencies in Table 2, the corresponding RGA matrices are

$$\lambda_{ij,first} = \begin{bmatrix} 1.00498 & -4.98120 \times 10^{-3} \\ -4.98120 \times 10^{-3} & 1.00498 \end{bmatrix}, \tag{12}$$

and

$$\lambda_{ij,second} = \begin{bmatrix} 1.00133 & -1.33774 \times 10^{-3} \\ -1.33774 \times 10^{-3} & 1.00133 \end{bmatrix}. \tag{13}$$

The results of equations (11), (12), and (13) lead us to conclude that the input-output variables of PLPS plant are almost decoupled. Accordingly, they motivate us to design a decentralized controller which provides the desired closed-loop characteristics. The decentralized controller design mainly consists of independent controller subsystems and exhibits several advantages including flexibility in operation, failure tolerance, simplified design, and tuning over a fully multivariable design (Campo and Morari 1994). With the consideration on the dynamics of PLPS, we design an independent single input-single output (SISO) controller in each loop.

4. CONTROLLER DESIGN

As shown in Figure 4, Figure 5, and Table 2, the PLPS has two mechanical resonances. On the other hand, the sensitivity of the overall system is required to be less than -10 dB at 20 Hz. This means that the closed-loop bandwidth frequency ω_{BW} should be larger than about 80 Hz. We can see that the frequencies associated with mechanical resonance are close to the desired closed-loop frequency ω_{BW}.

In general, it is necessary to take the bending modes into account when designing a control loop. A classical method of doing this is to introduce a notch filter (Jin and Kim 2008). Thus, we are going to pre-compensate for the oscillatory modes by introducing such a notch filter as the first step in the design procedure.

According to the analysis in the previous section, the continuous-time controller for each individual loop will be designed since the interaction is small enough to neglect. In the third step, the corresponding digital controller will be determined.

4.1. Notch Filter Design

In order to compensate for the two resonant modes of PLPS, the following type of 4th order notch filter is introduced in each loop.

$$F_i(s) = \frac{H(s)}{K(s)} = \frac{s^2 + 2\xi_{n1}\omega_{10}^s + \omega_{10}^2}{s^2 + 2\xi_{d1}\omega_{10}^s + \omega_{10}^2} \cdot \frac{s^2 + 2\xi_{n2}\omega_{20}^s + \omega_{20}^2}{s^2 + 2\xi_{d2}\omega_{20}^s + \omega_{20}^2} \quad \text{for } i = x, y, \tag{14}$$

where (ξ_{n1}, ω_{10}) and (ξ_{n2}, ω_{20}) are the first and the second oscillatory modes in Table 2, respectively. If we take the stability margins into account, the relative damping ratios of $F_x(s)$ for the x-axis loop and $F_y(s)$ for the y-axis loop were set to 0.1. That is, $\xi_{d1} = \xi_{d2} = 0.1$ for both $F_x(s)$ and $F_y(s)$. Figure 6 shows the bode plot of $F_x(s)G_{11}(s)$ which is the x-axis model $G_{11}(s)$ cascaded with the 4th order notch filter $F_x(s)$.

Here, we define $F_x(s)G_{11}(s)$ as the plant of the x-axis loop by

$$\begin{aligned} G_x(s) &= \frac{M(s)}{Q(s)} = \frac{N_{11}(s)}{D_{11}(s)} \frac{H(s)}{K(s)} \\ &= \frac{p_7 s^7 + p_6 s^6 + \cdots + p_1 s + p_0}{s^{10} + q_9 s^9 + \cdots + q_1 s + q_0}. \end{aligned} \tag{15}$$

Table 2. Bending modes of the identified models

	Bending modes			
	1st mode		2nd mode	
Model	ξ_{n1}	ω_{10}	ξ_{n2}	ω_{20}
$\widehat{G}_{11}(s)$	0.031	186.21 Hz	0.013	372.42 Hz
$\widehat{G}_{12}(s)$	0.0211	185.34 Hz	0.0028	381.32 Hz
$\widehat{G}_{21}(s)$	0.0173	190.02 Hz	0.0006	384.86 Hz
$\widehat{G}_{22}(s)$	0.033	202.13 Hz	0.015	416.98 Hz

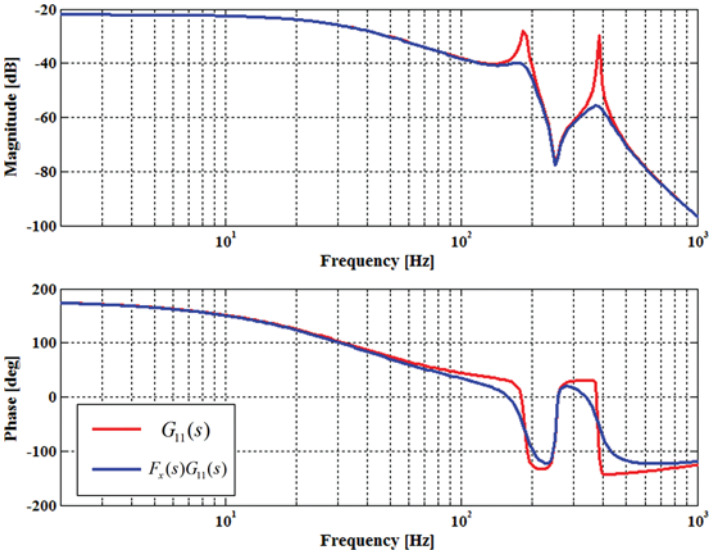

Figure 6. Bode plots of $G_{11}(s)$ and $F_x(s)G_{11}(s)$.

4.2. Continuous-Time Controller Design

In this step, we first try to design an SISO controller for the x-axis loop without regard to the effect of the y-axis loop. Similarly, another controller will be designed for the y-axis loop. For the sake of simplicity, we only describe the x-axis loop design here as shown in Figure 7.

Also we choose the following 3rd order controller:

$$C_x(s) = \frac{B_x(s)}{A_x(s)} = \frac{d_2 s^2 + d_1 s + d_0}{s(s^2 + c_1 s + c_0)}. \tag{16}$$

Then the closed-loop transfer function is given by

$$\begin{aligned} T_x(s) &= \frac{L_x(s)N_{11}(s)H(s)}{A_x(s)Q(s) + M(s)B_x(s)} \\ &= \frac{L_x(s)N_{11}(s)H(s)}{\delta_x(s)}. \end{aligned} \tag{17}$$

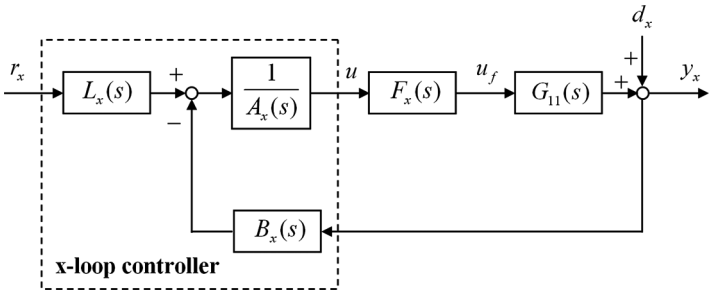

Figure 7. A decentralized controller in two-parameter configuration for the x-axis loop.

The characteristic polynomial $\delta_x(s)$ is

$$\begin{aligned}\delta_x(s) &= A_x(s)Q(s) + B_x(s)M(s) \\ &= s^{13} + \delta_{12}s^{12} + \cdots + \delta_1 s + \delta_0.\end{aligned} \tag{18}$$

The sensitivity transfer function is

$$S_x(s) = \frac{A_x(s)D_{11}(s)K(s)}{A_x(s)Q(s) + B_x(s)M(s)}. \tag{19}$$

Now, the problem is to find a low order controller of equation (16) that satisfies the design objectives to the augmented plant of equation (15). Recall that the main performance specification is that the sensitivity of the controller remains less than -10 dB at 20 Hz. Since $S_x + T_{xc} = 1$ (where $T_{xc}(s)$ is the complementary sensitivity function), the problem of obtaining a desirable sensitivity function $S_x^*(s)$ is equivalent to that of finding the corresponding $T_{xc}^*(s)$ (Kim et al. 2007). However, $T_{xc}(s)$ includes $B_x(s)$ in its numerator, so the problem may be complicated.

Instead of using $T_{xc}^*(s)$, we need to find the target closed-loop transfer function $T_x^*(s)$ that corresponds to S_x^*. It is not difficult to synthesize such a desirable $T_x^*(s)$. In this article, a previous approach (Keel et al. 2008) based on characteristic ratios and a generalized time constant was used for the generation of the target transfer function.

Thus, we suppose that such a target transfer function, $T_x^*(s)$, has already been determined. Now, the remaining task is to obtain a controller such that $T_x(s)$ matches $T_x^*(s)$. However, it is evident that this problem cannot be solved analytically because the solution does not exist due to the low order of the controller. In this article, we apply the partial model matching (PMM) method of Jin and Kim (2008) that uses the non-convex optimization technique.

We define the target transfer function as follows:

$$T_x^*(s) = \frac{N_{11}(s)H(s)L(s)}{\delta_x^*(s)}. \tag{20}$$

It is noted by Chen (1993) that $L_x(s)$ can always be determined independently of the feedback controllers $A_x(s)$ and $B_x(s)$. Since $N_{11}(s)$ and $H(s)$ are known, it is sufficient that only $\delta_x^*(s)$ in $T_x^*(s)$ is determined. Such a $\delta_x^*(s)$ can be constructed by using the so called *K-polynomial* (Keel et al. 2008). Let the vector of the controller parameters be

$$x = [\, c_1 \quad c_0 \quad d_2 \quad d_1 \quad d_0 \,]^T, \tag{21}$$

and the coefficient vectors, $\delta(s)$ and $\delta^*(s)$, be denoted as

$$\delta_x(x) := [\, \delta_{13} \quad \delta_{12} \quad \cdots \quad \delta_1 \quad \delta_0 \,]^T, \tag{22}$$

$$\delta_x^* := \left[\, \delta_{13}^* \quad \delta_{12}^* \quad \cdots \quad \delta_1^* \quad \delta_0^* \,\right]^T. \tag{23}$$

Then the coefficient vector of the characteristic polynomial, $\delta_x(s)$, can be expressed as a function of x, that is,

$$\delta_x(x) = Px + \gamma, \tag{24}$$

$$\text{where P} = \begin{bmatrix} 1 & 0 & 0 & 0 & 0 \\ q_9 & 1 & 0 & 0 & 0 \\ q_8 & q_9 & 0 & 0 & 0 \\ \vdots & q_8 & p_7 & 0 & 0 \\ q_1 & \vdots & \vdots & p_7 & 0 \\ q_0 & q_1 & p_0 & \vdots & p_7 \\ 0 & q_0 & 0 & p_0 & \vdots \\ 0 & 0 & 0 & 0 & p_0 \end{bmatrix}, \ \gamma = \begin{bmatrix} q_9 \\ q_8 \\ \vdots \\ q_1 \\ q_0 \\ 0 \\ 0 \\ 0 \end{bmatrix}.$$

Now we define the cost function as follows:

$$\begin{aligned} f_0(x) :&= [\delta_x(x) - \delta_x^*]^T[\delta_x(x) - \delta_x^*] \\ &= [Px + r - \delta_x^*]^T[Px + r - \delta_x^*] \\ &= x^T(P^TP)x - 2(r - \delta_x^*)^TPx + [(r - \delta_x^*)^T(r - \delta_x^*)]. \end{aligned} \tag{25}$$

The PMM problem can be regarded as an LSE problem in the sense that $f_0(x)$ is minimized with respect to x. In other words, the control design problem associated with PMM has been reduced to an LSE problem, as follows:

$$x_o^* = \min_x f_0(x). \tag{26}$$

It was pointed out by Kim et al. (2003) that the coefficients of relatively lower powers of s in a transfer function are dominantly related to the step response. For example, among δ_is, δ_0, δ_1, δ_2, δ_3 have more effect on the step response than δ_{n-2}, δ_{n-1}, δ_n.

Note that the solution x_o^* does not guarantee closed-loop stability. Therefore, the stability condition must also be imposed on this objective function. Since it is very difficult to apply the Routh-Hurwitz criterion directly, we are obliged to employ the sufficiency condition for stability developed by Lipatov and Sokolov (1979). It states that the polynomial from equation (18) is stable if the following inequalities hold:

$$\delta_k\delta_{k+1} \geq 1.4656^2\delta_{k-1}\delta_{k-2}, \quad \text{for } k = 1, 2, \cdots, n-2. \tag{27}$$

The above stability condition can be expressed in terms of a matrix and vectors as follows:

$$f_k(x) = x^TA_kx + 2b_k^Tx + c_k \geq 0, \quad \text{for } k = 1, 2, \cdots, n-2 \tag{28}$$

where

$$\begin{aligned} A_k &= p_{k+1}^T p_k - \eta p_{k+2}^T p_{k-1}, \\ b_k &= \frac{1}{2}[(\gamma_k p_{k+1} + \gamma_{k+1} p_k) - \eta(\gamma_{k-1} p_{k+2} + \gamma_{k+2} p_{k-1})], \\ c_k &= \gamma_k \gamma_{k+1} - \eta \gamma_{k-1} \gamma_{k+2}, \end{aligned} \tag{29}$$

$$P = [\, p_0 \quad p_1 \quad \cdots \quad p_{n-1} \quad p_n \,]^T.$$

Therefore, the problem of designing a fixed, lower-order controller with guaranteed stability is reduced to the following global optimization.

$$x^* = \min_x f_0(x) \tag{30}$$

subject to $f_k(x) \geq 0$ for $k = 1, 2, \ldots, n-2$.

As shown by Jin and Kim (2008), a Matlab solver is available for solving the non-convex optimization problem in equation (30). Applying the approach in Keel et al. (2008) to the construction of $T_x^*(s)$, we have obtained a target $T_c^*(s)$ with the chosen values of $\alpha_1 = 2.0078$ and $\tau = 0.0078$ sec. The coefficient vector of the resulting $\delta_x^*(s)$ in $T_x^*(s)$ is

$$\begin{aligned} \delta_x^* = [\, & 1 \quad 9.247 \times 10^3 \quad 4.2587 \times 10^7 \quad 1.2896 \times 10^{11} \\ & 2.8583 \times 10^{14} \quad 4.8891 \times 10^{17} \quad 6.6325 \times 10^{20} \quad 7.2215 \times 10^{23} \\ & 6.3109 \times 10^{26} \quad 4.3740 \times 10^{29} \quad 2.3395 \times 10^{32} \quad 9.1592 \times 10^{34} \\ & 2.3577 \times 10^{37} \quad 3.0226 \times 10^{39} \,]. \end{aligned} \tag{31}$$

The values for $T_y^*(s)$ have been chosen as $\alpha_1 = 1.9900$ and $\tau = 0.0069$ sec. Finally, the controllers for both the x-axis and y-axis loops are determined by using the Gloptipoly (Jin and Kim 2008) which are shown in Table 3.

Now, the remaining design problem is to find a $L_x(s)$. It is well known that the closed-loop system must be Type-1 in order to achieve the zero steady state error to the step reference. A simple way to do this is to make $T_x(0) = 1$. Therefore, from equation (17),

$$L_x(s) = l_0 = \frac{\delta_x(0)}{N_{11}(s)H(0)} = d_0. \tag{32}$$

Table 3. Continuous-time controller gains

Gain	$C_x(s)$	$C_y(s)$
c_1	3.71577×10^7	5.65019×10^7
c_0	1.77476×10^{10}	7.54170×10^9
d_2	7.97667×10^7	9.17117×10^7
d_1	3.91655×10^{10}	2.93930×10^{10}
d_0	4.39249×10^{12}	2.47080×10^{12}

4.3. Digitizing the Continuous-Time Controller

In this step, by applying the Tustin approximation (Astrom and Wittenmark 1997) to the designed continuous-time controllers and notch filters, we obtain the digital controllers with a sampling frequency of 3 kHz. The structure of the digital controller is represented by

$$\begin{aligned} z(k+1) &= A_D z(k) + B_D e(K) \\ u(k) &= C_D z(k) + D_D e(k), \end{aligned} \tag{33}$$

where

$$\begin{aligned} z(k+1) &= [\, z_1(k+1) \quad z_2(k+1) \quad z_3(k+1) \,], \\ z(k) &= [\, z_1(k) \quad z_2(k) \quad z_3(k) \,], \\ e(k) &= [\, r(k) \quad y(k) \,], \end{aligned}$$

$u(k)$ is the control input, and A_D, B_D, C_D, D_D are the gains of the digital controller.

The gains of the digital controller for the x-axis channel are as follows:

$$A_D = \begin{bmatrix} -0.4524 & 9.1263 \times 10^{-5} & 1.5211 \times 10^{-8} \\ -1.2441 \times 10^{3} & 0.7926 & 2.9878 \times 10^{-4} \\ 0 & 0 & 1 \end{bmatrix},$$

$$B_D = \begin{bmatrix} 58.4472 & -2.4376 \times 10^{4} \\ 1.1481 \times 10^{6} & 5.4393 \times 10^{6} \\ 7.6851 \times 10^{9} & -7.6851 \times 10^{9} \end{bmatrix}, \tag{34}$$

$$\begin{aligned} C_D &= \begin{bmatrix} 9.1263 \times 10^{-5} & 1.5211 \times 10^{-8} & 2.5351 \times 10^{-12} \end{bmatrix}, \\ D_D &= \begin{bmatrix} 9.7412 \times 10^{-3} & -4.0627 \end{bmatrix} \end{aligned}$$

For the y-axis channel, the controller gains are given by

$$A_D = \begin{bmatrix} -2.6237 & 1.2294 \times 10^{-4} & 2.0489 \times 10^{-8} \\ -8.1447 \times 10^{2} & 0.8643 & 3.1071 \times 10^{-4} \\ 0 & 0 & 1 \end{bmatrix},$$

$$B_D = \begin{bmatrix} 4.0839 & -1.5677 \times 10^{4} \\ 6.1929 \times 10^{5} & -7.7757 \times 10^{6} \\ 3.9863 \times 10^{9} & -3.9863 \times 10^{9} \end{bmatrix}, \tag{35}$$

$$\begin{aligned} C_D &= \begin{bmatrix} 1.2294 \times 10^{-4} & 2.0489 \times 10^{-8} & 3.4149 \times 10^{-12} \end{bmatrix}, \\ D_D &= \begin{bmatrix} 6.8065 \times 10^{-3} & -2.6129 \end{bmatrix}. \end{aligned}$$

Also, the discrete form of the notch filter is represented as

$$NF(z) = \frac{H(z)}{K(z)} = \frac{dh_4 z^4 + dh_3 z^3 + dh_2 z^2 + dh_1 z + dh_0}{z^4 + dk_3 z^3 + dk_2 z^2 + dk_1 z + dk_0}. \tag{36}$$

Then the gains of the notch filter for the x-axis channel are as follows:

$$\begin{bmatrix} dh_4 \\ dh_3 \\ dh_2 \\ dh_1 \\ dh_0 \end{bmatrix} = \begin{bmatrix} -0.9218 \\ -3.0303 \\ 4.2647 \\ -2.9692 \\ -0.8839 \end{bmatrix}, \begin{bmatrix} dk_3 \\ dk_2 \\ dk_1 \\ dk_0 \end{bmatrix} = \begin{bmatrix} -3.1631 \\ 4.2603 \\ -2.8365 \\ -0.8096 \end{bmatrix}. \tag{37}$$

For y-axis channel, the gains of the notch filter are

$$\begin{bmatrix} dh_4 \\ dh_3 \\ dh_2 \\ dh_1 \\ dh_0 \end{bmatrix} = \begin{bmatrix} -0.9177 \\ -2.888 \\ 4.0147 \\ -2.8186 \\ -0.8732 \end{bmatrix}, \begin{bmatrix} dk_3 \\ dk_2 \\ dk_1 \\ dk_0 \end{bmatrix} = \begin{bmatrix} -3.0231 \\ 4.0097 \\ -2.6843 \\ -0.7960 \end{bmatrix}. \tag{38}$$

5. EXPERIMENTAL RESULTS

In this section, the experimental evaluations will be shown. The experimental setup including PLPS and controller is shown in Figure 8. The digitized controllers and notch filters are implemented on an M6x DSP board. The detailed hardware specifications for each module are listed in Table 4.

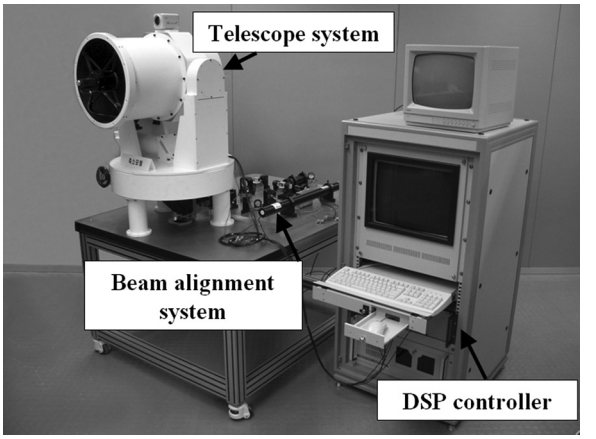

Figure 8. Experimental setup.

Table 4. Hardware specifications

Symbol	Specification	Manufacturer
DSP control board	M6x	Innovative Integration Co.
FSM platform	S-340.AL Unloaded resonant frequency: 1.4 kHz ± 20% Resonant frequency w/Ø75 × 22 mm glass mirror: 0.4 kHz ± 20%	Physik Instrumente Co.
Power amplifier	2-channel E-505	
Anti-aliasing Filter/ Amp	1-channel E-505	
Beam Alignment Sensing System	E-509	
AD/DA converters	16 bit A4D4 module	Piggyback Co.

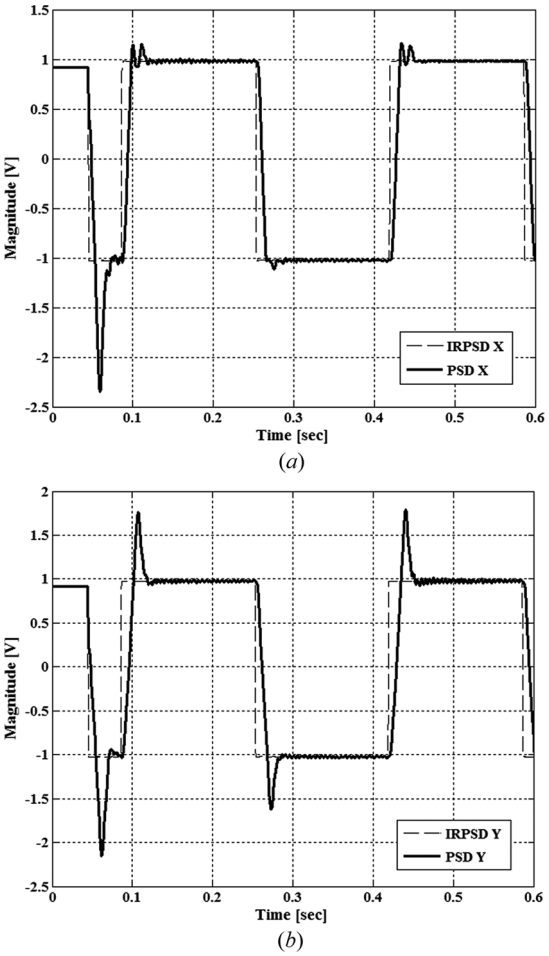

Figure 9. IRPSD and PSD signals (*a*) x axis (*b*) y axis.

The experiment is composed of two different tests. One observes the transient responses of the PLPS when square-wave command signals of $\pm 1 V_{pp}$ were excited into both axes of the PLPS system simultaneously. The other obtains the sensitivity responses of PLPS using an Agilent 35670A.

The results of the first test, namely, the command signals and their responses on each axis, are shown in Figure 9*a* and Figure 9*b*. Also, the control input signals are shown in Figure 10*a* and Figure 10*b*. The time response specifications for transient behavior are summarized in Table 5. The results show that, when the control input is generated within a span of 10 volts, the designed controller maintains the stability of PLPS and the output responses of PLPS track the command signals without steady-state errors.

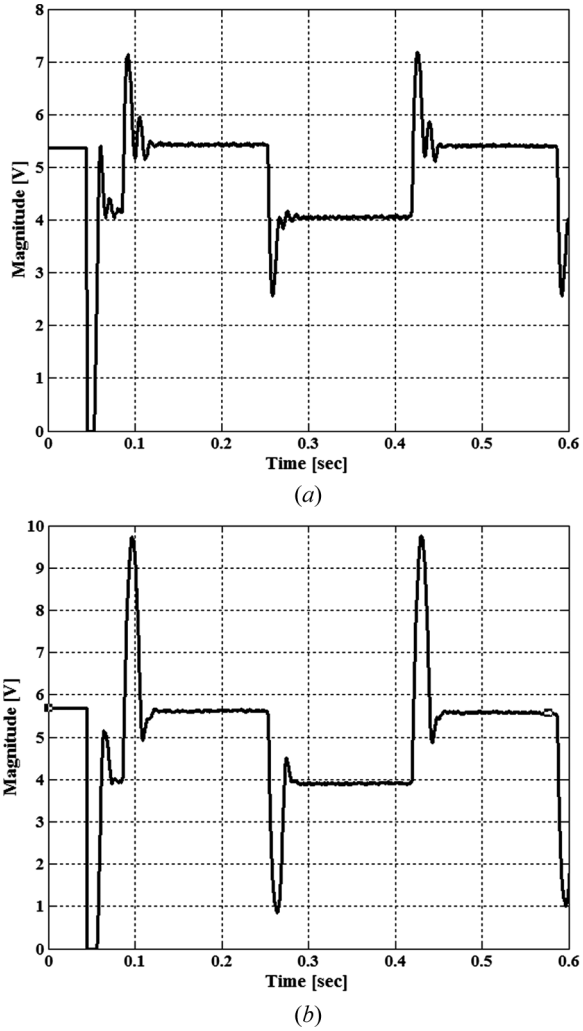

Figure 10. Control input signals (*a*) x axis (*b*) y axis.

Table 5. Time response specifications

Transient response	X axis	Y axis
Overshoot	14.20%	75.75%
Settling time	0.034 sec	0.0406 sec
Rise time	0.0074 sec	0.0103 sec
Delay time	0.0083 sec	0.0105 sec
Steady state error	≈0	≈0
Span of control input signal	0 ~ 7.144 V	0 ~ 9.737 V

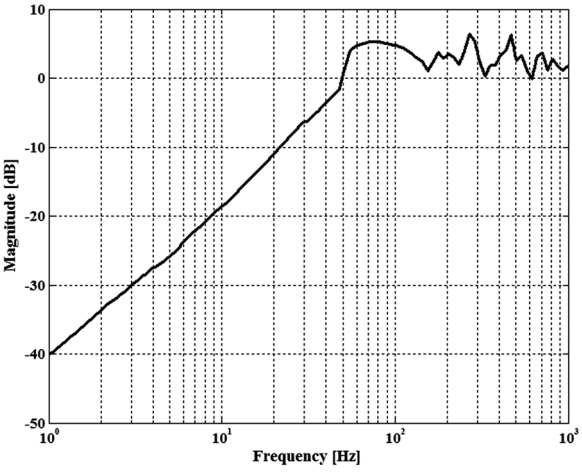

(*a*)

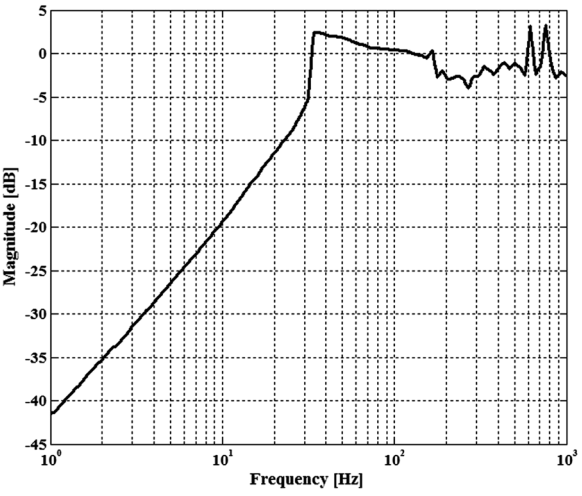

(*b*)

Figure 11. Sensitivity responses (*a*) x axis (*b*) y axis.

Table 6. Frequency response specifications

		X axis	Y axis
Sensitivity margin	At 15 Hz	−14.163 dB	−14.708 dB
	At 30 Hz	−6.3473 dB	−6.165 dB
Maximum peak		6.44405 dB (at 270 Hz)	3.21187 dB (at 758 Hz)

In the second test, by using an Agilent 35670A, we measured the frequency response on each axis according to equation (19). Figure 11*a* and Figure 11*b* show the obtained sensitivity responses of the PLPS. The system has a sensitivity margin of −10.842 dB at 20 Hz on the x-axis, and −11.433 dB at 20 Hz on the y-axis as listed in Table 6. Lastly, to assess the robustness of PLPS, we adopted the concept of vector margin as a performance measure. The vector margin is defined as the inverse of sensitivity function and represents the distance from a point on the Nyquist curve of the loop-transfer function to the critical point −1 (Smith 1958). To have a reasonable robustness against instability, the largest value of sensitivity data should not be too large. A typical requirement is $|S(j\omega)|_{\max} < 2 (\leq 6\text{dB})$ (Landau and Zito 2006).

From the maximum peak of sensitivity responses in Table 6, we calculate $|S_x(j\omega)|_{\max} = 2.0999$ and $|S_y(j\omega)|_{\max} = 1.4474$. Therefore, the vector margin on x-axis loop is 0.4762 and 0.6908 on y-axis loop. These margins indicate implicitly that the designed PLPS has a moderate robustness on both axes.

6. CONCLUSION

A comprehensive control strategy was applied to the design of a decentralized digital controller, so that PLPS had the ability to track the command signals quickly and reject undesirable disturbances. The strategy includes all steps ranging from data acquisition to controller design to implementation in an actual system. By applying the controller to an actual PLPS system, we evaluated the controller's performance. The experimental results showed that the controller satisfied the given sensitivity requirement.

A weighted least square algorithm is used to identity a mathematical model for PLPS. The RGA analysis of this PLPS model justifies our adoption of a decentralized controller design scheme. Before we design the controller, a notch filter is added to diminish the effects of bending modes. Also, the partial model matching method was used to find a continuous-time controller which satisfies the given specification for disturbance rejection. The digital controller is obtained by applying the Tustin approximation. Finally, the parameters of the controller are implemented to the M6x DSP board in the experimental environment.

By means of two experiments, we evaluated the transient response specifications of the controller and its ability to reject disturbance signals. It has sensitivity margins of −10.842 dB at 20 Hz on the X axis, and −11.433 dB at 20 Hz on the Y axis. Also the span of control input is within the limits of 10 V. The vector margins were measured to be 0.4762 on the x-axis loop and 0.6908 on the y-axis loop. These results show that the strategy employed in this article was successful in designing the PLPS that satisfies the given performance and stability requirements.

APPENDIX

The Parameters of the Identified Model

The parameters of the model identified in equation (2) are listed below. (Only six ciphers are included due to limited space.)

$$\widehat{G}_{11}(s) = \begin{bmatrix} b_3 \\ b_2 \\ b_1 \\ b_0 \end{bmatrix} = \begin{bmatrix} 4.777343 \times 10^{7} \\ 2.317778 \times 10^{11} \\ 1.085097 \times 10^{14} \\ 4.799981 \times 10^{17} \end{bmatrix}, \begin{bmatrix} a_5 \\ a_4 \\ a_3 \\ a_2 \\ a_1 \\ a_0 \end{bmatrix} = \begin{bmatrix} 6.206951 \times 10^{2} \\ 6.975666 \times 10^{6} \\ 3.825860 \times 10^{9} \\ 8.095653 \times 10^{12} \\ 3.693430 \times 10^{15} \\ 3.318528 \times 10^{17} \end{bmatrix}$$

$$\widehat{G}_{12}(s) = \begin{bmatrix} b_3 \\ b_2 \\ b_1 \\ b_0 \end{bmatrix} = \begin{bmatrix} -2.52486 \times 10^{6} \\ -1.34233 \times 10^{10} \\ -6.95876 \times 10^{12} \\ -3.30155 \times 10^{16} \end{bmatrix}, \begin{bmatrix} a_5 \\ a_4 \\ a_3 \\ a_2 \\ a_1 \\ a_0 \end{bmatrix} = \begin{bmatrix} 4.99341 \times 10^{2} \\ 7.17809 \times 10^{6} \\ 3.40316 \times 10^{9} \\ 8.29473 \times 10^{12} \\ 3.41578 \times 10^{15} \\ 4.15091 \times 10^{17} \end{bmatrix}$$

$$\widehat{G}_{21}(s) = \begin{bmatrix} b_3 \\ b_2 \\ b_1 \\ b_0 \end{bmatrix} = \begin{bmatrix} -3.95098 \times 10^{6} \\ -3.35113 \times 10^{9} \\ -1.25106 \times 10^{13} \\ -7.77024 \times 10^{15} \end{bmatrix}, \begin{bmatrix} a_5 \\ a_4 \\ a_3 \\ a_2 \\ a_1 \\ a_0 \end{bmatrix} = \begin{bmatrix} 2.97515 \times 10^{2} \\ 7.31722 \times 10^{6} \\ 2.08941 \times 10^{9} \\ 8.63673 \times 10^{12} \\ 2.11907 \times 10^{15} \\ 2.73683 \times 10^{17} \end{bmatrix}$$

$$\widehat{G}_{22}(s) = \begin{bmatrix} b_3 \\ b_2 \\ b_1 \\ b_0 \end{bmatrix} = \begin{bmatrix} 4.65266 \times 10^{7} \\ 2.57761 \times 10^{11} \\ 1.72295 \times 10^{14} \\ 7.66253 \times 10^{17} \end{bmatrix}, \begin{bmatrix} a_5 \\ a_4 \\ a_3 \\ a_2 \\ a_1 \\ a_0 \end{bmatrix} = \begin{bmatrix} 7.58831 \times 10^{2} \\ 8.65724 \times 10^{6} \\ 5.75235 \times 10^{9} \\ 1.20227 \times 10^{13} \\ 6.60198 \times 10^{15} \\ 7.06706 \times 10^{17} \end{bmatrix}$$

ACKNOWLEDGMENT

This research was supported by the Basic Science Research Program through the National Research Foundation of Korea (NRF) funded by the Ministry of Education, Science and Technology (grant number: 2010-0021082).

REFERENCES

Astrom, K. J. and B. Wittenmark. 1997. *Computer-controlled systems: Theory and Design*. Upper Saddle River, New Jersey, USA: Prentice-Hall.

Bristol, E. H. 1966. On a new measure of interaction for multivariable process control. *IEEE Transactions on Automatic Control* 11 (1): 133–134.

Campo, Peter J. and Manfred Morari. 1994. Achievable closed-loop properties of systems under decentralized control: conditions involving the steady-state gain. *IEEE Transactions on Automatic Control* 39 (5): 932–943.

Chen, Chi Tsong. 1993. *Analog and digital control system design: Transfer-function, state-space, and algebraic methods*. New York, USA: Saunders College Publishing.

Franklin, Gene F., J. David Powell, and Michael L. Workman. 1997. *Digital control of dynamic systems*. Boston, USA: Addison-Wesley.

Jin, Li Hua, and Young Chol Kim. 2008. Fixed, low-order controller design with time response specifications using non-convex optimization. *ISA Trans.* 47 (4): 429–438.

Keel, L. H., Young Chol Kim, and S. P. Bhattacharyya. 2008. Ch. 6 Transient response control. *Lecture Note on the 17th IFAC World Congress Tutorial Workshop on Advances in Three Term Control*. Seoul, Korea: July.

Kim, Young Chol, L. H. Keel, and S. P. Bhattacharyya. 2003. Transient response control via characteristic ratio assignment. *IEEE Transactions on Automatic Control* 48 (12): 2238–2244.

Kim, Young Chol, L. H. Keel, and S. P. Bhattacharyya. 2007. Computer aided control system design: Multiple design objectives. *Proceedings of the European Control Conference* 512–517.

Kuang, Jiagming, Tao Tang, Chengyu Fu, Ke Ding., and Wei Yu. 2009. Simulation of the fast steering mirror control system based on gyro velocity feedback. *Proceedings of the SPIE* 7508: 75080Z–75080Z9.

Landau, D. Ioan and Gianluca Zito. 2006. *Digital control systems design identification and implementation*. London, England: Springer-Verlag.

Lipatov, A. V. and N. I. Sokolov. 1979. Some sufficient conditions for stability and instability of continuous linear stationary systems. *Automation and Remote Control* 39: 1285–1291.

Orzechoski, Pawel Konrad, James Steven Gibson, Tsu-Chin Tsao, Dan Herrick, and Victor Beazel. 2008b. Nonlinear adaptive control of optical jitter with a new liquid crystal beam steering device. *American Control Conference*, June: 4185–4190.

Orzechoski, Pawel Konrad, Neil Yinan Chen, James Steven Gibson, and Tsu-Chin Tsao. 2008a. Optimal suppression of laser beam jitter by high-order RLS adaptive control. *IEEE Transactions on Control Systems Technology* 16 (2): 255–267.

Schwartz, Joseph, Gerald T. Wilson., and Joel Avidor. 2002. Tactical high energy laser. *Proceedings of SPIE on Laser and Beam Control Technologies* 4632: 10–20.

Shinsky, F. G. 1981. *Controlling multivariable processes*. Research Triangle Park, USA: Instrument Society of America.

Skormin, V. A., T. E. Busch, and M. A. Givens. 1995. Model reference control of a fast steering mirror of a pointing, acquisition and tracking system for laser communications. *Proceedings of the National Aerospace and Electronics Conference* 2: 907–913.

Smith, Otto J. M. 1958. *Feedback control systems*. New York, USA: McGraw-Hill.

Sweeney, Michael N., Gerald A. Rynkowski, Mehrdad Ketabchi, and Robert Crowley. 2002. Design considerations for fast-steering mirrors (FSMs). *Proceedings of SPIE* 4773: 63–73.

Zhou, Qingkun, Pinhas Ben-Tzvi, and Dapeng Fan. 2009. Design and analysis of a fast steering mirror for precision laser beams steering. *Sensors & Transducers Journal* 5: 104–118.